

# Solvent Tunable Optical Properties of a Polymerized Vinyl- and Thienyl-Substituted Ionic Liquid<sup>†</sup>

Gregory A. Becht,<sup>†</sup> Sungwon Lee,<sup>†</sup> Sönke Seifert,<sup>‡</sup> and Millicent A. Firestone\*,<sup>†</sup>

Materials Science and X-ray Sciences Divisions, Argonne National Laboratory, 9700 South Cass Avenue, Argonne, Illinois 60439

Received: March 31, 2010; Revised Manuscript Received: August 29, 2010

Thermal free radical polymerization of a self-assembled, bifunctional imidazolium-based ionic liquid (IL) monomer bearing both vinyl and thienyl groups is reported. FT-IR spectroscopy proves that the polymerization occurs through both the vinyl and thienyl groups. The polymer is resistant to swelling in water and common organic solvents. The as-synthesized polymer can be readily chemically doped and de-doped. Small-angle X-ray scattering studies indicate that the dried polymer adopts a weakly ordered lamellar structure. The p-doped, ethanol-solvated polymer undergoes a structural conversion to a nonlamellar phase. The absorption and photoluminescence spectra can be modulated in both the neutral (thiophene) and p-doped states depending on whether the polymer is dry or ethanol-solvated. The results demonstrate the possibility of incorporating solvent responsive optical characteristics in a  $\pi$ -conjugated polymer.

## Introduction

The optoelectronic properties of conjugated polymers are of increasing interest for potential application in a variety of technologies, including the fabrication of polymer light-emitting devices (PLEDs).<sup>1</sup> Traditionally, polythiophene has not been considered well suited for use as an emissive layer because of its low quantum yield. The fluorescence efficiency of polythiophenes are typically on the order of ~40% in solution but plummets to less than 2% in the solid state.<sup>2</sup> Nonradiative decay from strong interchain interactions and intersystem crossing are attributed to the loss of efficiency in the solid, thin film state. One promising approach for inhibiting interchain interactions has been the incorporation of bulky alkyl side chains.<sup>3</sup> In addition to intermolecular effects, the absorption and emission properties of the polymers are also strongly influenced by the conjugation length and conformational state (effective conjugation length) of the polymer backbone. To further improve the photophysical properties of conjugated polymers for use as components in optoelectronic devices better control over both intra- and intermolecular interactions through molecular engineering is required.<sup>2</sup> It is anticipated that through appropriate molecular design, external control over the assembled structure would permit active regulation of the optical and photophysical properties, perhaps leading to the development of tunable or stimuli-responsive  $\pi$ -conjugated systems.

Polyalkylthiophenes can undergo chromism, demonstrating striking color changes upon the association or binding of molecules (affinitychromism) or ions (ionchromism).<sup>4</sup> The chromic behavior arises from conformational changes in the polymer backbone, typically from a planar to a nonplanar state. Polyelectrolyte derivatives of polyalkylthiophenes have been shown to bind or adsorb a variety of biomolecules upon which a direct read out is obtained by monitoring the spectral signal.<sup>5</sup> While many of these studies have proven useful for sensing

and monitoring applications few studies have looked at reversible binding and hence reversibility in the optical properties. Alternatively, the possibility of triggering alterations in polymer conformation in response to temperature (thermochromism)<sup>6</sup> or solvent quality changes (solvatochromism)<sup>6,7</sup> have also been reported. Frequently the conformational changes cause an alteration in the effective conjugation length inducing optical shifts in the absorption spectrum. Solvent changes have also been shown to induce alterations in intermolecular interactions (e.g., excitons or  $\pi-\pi$  interactions), leading to changes in both the absorption and emission spectra. These reports suggest the possibility of devising  $\pi$ -conjugated polymers that undergo reversible structural changes in response to various environmental factors that may elicit changes in polymer optical characteristics.

In prior work, we have demonstrated the polymerization of self-assembled, lyotropic liquid-crystalline phases of ionic liquid monomers to form nanostructured durable self-supporting polymers.<sup>8–11</sup> Several of these polymers also exhibited solvent dependent structural changes.<sup>8,10</sup> Specifically, we used the solvent induced adjustability in polymer architecture to regulate the internal packing arrangement of in situ synthesized gold nanoparticles, proving that the collective optical response (surface plasmon resonance) could be modulated by architecture.<sup>10</sup> More recently, we have sought to incorporate moieties that would impart an electronic component to these polymers by introduction of a thienyl group on the terminus of a C<sub>10</sub> alkyl chain of a methyl imidazolium-based ionic liquid.<sup>12</sup> The incorporation of an electronic component with an ionic liquid will also allow for the preparation of a mixed ionic and electronic conducting material. Oxidative polymerization yielded a low molecular weight polymer that adopted a random coil conformational state in aqueous solution. Replacement of the methyl group on the imidazolium with a vinyl moiety in conjunction with the alkyl-appended thiophene yielded a bifunctional monomer that was electropolymerized producing an electronically conducting polymer film.<sup>13</sup> In this report, we now evaluate the potential of polymerizing the same bifunctional monomer preorganized into a lyotropic mesophase using

<sup>†</sup> Part of the “Michael R. Wasielewski Festschrift”.

\* To whom correspondence should be addressed. Phone: 630-252-8298. Fax: 630-252-9151. E-mail: firestone@anl.gov.

<sup>†</sup> Materials Science.

<sup>‡</sup> X-ray Sciences Divisions.

thermal, free radical initiation as a means of forming a durable, self-supporting  $\pi$ -conjugated network polymer with solvent responsive optical properties.

## Experimental Section

**Materials and Reagents.** NMR solvents ( $D_2O$ , and  $CDCl_3$ ) and chemicals (sodium bisulfate, 3-bromo-4-methylthiophene, 10-bromo-1-decanol, 1-vinylimidazole, copper(I) bromide, iron(III) chloride, ammonium persulfate, 20% sodium methoxide in methanol, *N*-methylpyrrolidone, hexanes, ethyl acetate, dimethyl formamide, ethanol, dimethyl sulfoxide, toluene,  $\alpha,\alpha'$ -azodiisobutyramidine dihydrochloride (A1BA), and hydrazine) were used as received from Sigma-Aldrich (Milwaukee, WI). Diethyl ether, chloroform, acetonitrile, and methanol were used as received from Fisher Scientific (Pittsburgh, PA). The synthesis of the monomer, 1-(10-(4-methylthiophen-3-yloxy)-decyl)-3-vinylimidazolium bromide (1), was previously described in detail elsewhere.<sup>13</sup>

Polymerization of 1-(10-(4-methylthiophen-3-yloxy)decyl)-3-vinylimidazolium bromide (2) was carried out via thermal free radical polymerization using A1BA as the initiator. 1-(10-(4-methylthiophen-3-yloxy)decyl)-3-vinylimidazolium bromide (0.10 g, 0.23 mmol) and A1BA (2.00 mg, 0.007 mmol) in water (total water content was 18% (w/w)) was homogenized by vortex mixing in a vial. The reaction mixture was loaded in air into a borosilicate glass pipet (~2–3 in.) using negative pressure. It has been previously noted that polymerization of similar IL monomers do not appear to be inhibited by the presence of oxygen, which may be in part due to the poor solubility and slow diffusivity of oxygen in dialkylimidazolium ILs.<sup>8</sup> The sample was placed in an oven at 85 °C for 3 h. The resulting polymer was removed from the pipet by breaking the pipet glass with a razor blade. The recovered polymer was washed with nanopure  $H_2O$  and ethanol. The solid polymer was amber color. (ATR) FT-IR ( $cm^{-1}$ ): 3242, 3131, 3076, 2927, 2855, 1680, 1398, 1261, 1228, 1163, 1070, 881, 852, 770, 729.

The p-doped polymer (3) was obtained by treating the as-synthesized polymer (0.25 g, 0.58 mmol) with a 10 mL aqueous solution of  $FeCl_3$  (0.11 g, 0.58 mmol) under Ar flow at 25 °C for 4 h. After 4 h, a 10 mL aqueous solution of  $(NH_4)_2S_2O_8$  (0.13 g, 0.58 mmol) was added to the reaction mixture and stirred an additional 24 h. The recovered solid polymer segments were washed with copious amounts of nanopure  $H_2O$ . The resultant solid polymer was red in color. (ATR) FT-IR ( $cm^{-1}$ ): 3257, 3135, 3087, 2927, 2855, 1682, 1631, 1163, 1046, and 974 (signature modes for p-doped polymer), 884, 851, 768, 726.

The de-doped polymer (4) was obtained by treating the freshly p-doped polymer (0.25 g, 0.58 mmol) with a 10 mL solution of 1:1 hydrazine/ethanol under Ar flow at 25 °C for 15 h. The polymers were taken out of the solution, filtered and washed with copious amounts of ethanol. The resultant solid polymer was deep green in color. (ATR) FT-IR ( $cm^{-1}$ ): 3332, 3257, 3229, 3175, 3154, 2972, 2927, 2855, 1616, 1589 (signature mode for de-doped), 1393, 1089 (signature mode for de-doped), 1049, 1019, and 996 (signature modes for de-doped), 882, 853, 768, 725.

## Physical Methods

**Spectroscopy/Microscopy.** ATR-FT-IR spectroscopy was performed using a Bruker Vertex 70 spectrometer over the frequency range 4000–700  $cm^{-1}$ . Spectra were recorded at 4  $cm^{-1}$  resolution and averaged over 256 scans. UV-vis spectra were recorded from 200–900 nm using a Shimadzu UV mini 1240 spectrophotometer at a spectral resolution of 1 nm.

UV-vis-NIR spectra were recorded from 200–1200 nm using a Cary 5 spectrophotometer at a spectra resolution of 1 nm. Photoluminescence spectra were recorded using a Shimadzu RF-1501 spectrofluorophotometer. Polarized optical microscopy was performed on Baush & Lomb Micro Zoom microscope equipped with a custom-made Peltier temperature controller unit.

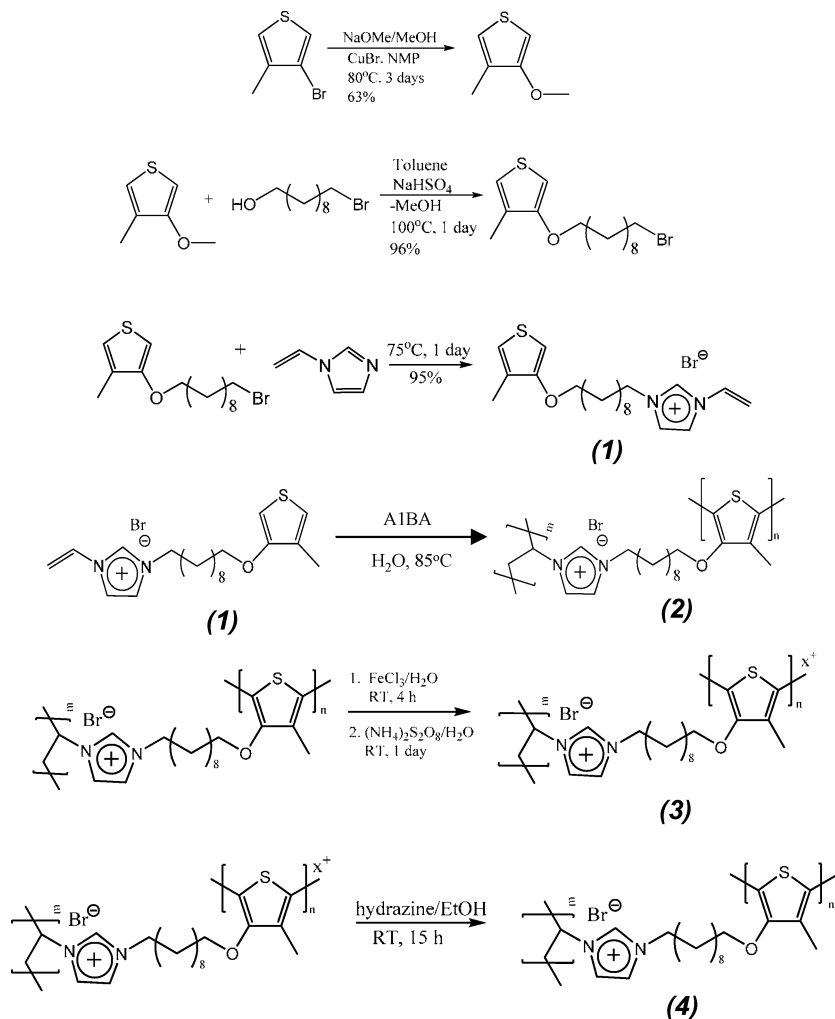
**Thermal Analysis.** Differential scanning calorimetry (DSC) was performed on a Q100 instrument (TA Instruments, New Castle, DE) interfaced with a refrigerated cooling system. Weighed amounts (1–5 mg) of the sample were sealed in aluminum pans and data were collected between –70 to 100 °C at a heating rate of 2 °C/min. Instrument calibration was performed using an indium standard. Thermogravimetric analysis (TGA) was carried out on a TA Instrument Q50 by heating a known amount of sample (1–5 mg) in a platinum pan from 20 °C to a final temperature of 400 °C at a rate of 10 °C/min under  $N_2$  flow.

**DC Conductivity.** Conductivity measurements were carried employing a two-probe technique using a HP digital multimeter (HP34410A, Agilent Technologies, Santa Clara, CA). The sample was held in a laboratory-built sealable Teflon cell equipped with two mirror-finished stainless steel electrodes (surface area = 0.071  $cm^2$ ). All measurements were conducted in a temperature-controlled chamber (TPS TUJR test chamber, White Deer, PA) at 25 ± 1 °C. Reported values were obtained by averaging the result from five different samples.

**X-ray Scattering.** Small-angle X-ray scattering (SAXS) measurements were made using the instrument at undulator beamline 12ID-C beamline (11–12 keV) of the Advanced Photon Source at Argonne National Laboratory. The 2D scattering profiles were recorded with a MAR-CCD-165 detector (Mar USA, Evanston, IL), which features a circular, 165 mm diameter active area and 2048 × 2048 pixel resolution. The sample-to-detector distance was such as to provide a detecting range for momentum transfer of  $0.001 \text{ \AA}^{-1} < q < 0.6 \text{ \AA}^{-1}$ . The scattering vector,  $q$ , was calibrated using a silver behenate standard at  $q = 1.076 \text{ \AA}^{-1}$ . The 2D scattering images were first corrected for spatial distortion and sensitivity of the detector and then radially averaged to produce plots of scattered intensity,  $I(q)$ , versus scattering vector,  $q$ , where  $q = 4\pi/\lambda(\sin \theta)$ . The value of  $q$  is proportional to the inverse of the length scale,  $\text{\AA}^{-1}$ . For these measurements, samples were probed either as freely suspended polymers or as the gels confined in glass capillaries. Measurements were made at 25 °C ( $\pm 1$  °C).

**Determination of Gel Fraction.** Freshly synthesized polymers were cut into cylindrical segments and weighed. Each piece was then fully immersed into methanol or xylene for 15 h. The solid polymer segments were removed from the solvent and dried under vacuum then weighed. The gel fraction was determined by taking a ratio of the final weight ( $W_f$ ) versus the initial weight ( $W_0$ ).<sup>14,15</sup>

**Solvent Studies.** Equilibrium swelling in various solvents was carried out on freshly synthesized polymer cut into cylindrical pieces with the dimensions 1.2–2.1 mm × 1.0 mm ( $L \times W$ ). Each piece was then fully immersed into one of the following solvents: hexanes (Hex), ethyl acetate (EtOAc), chloroform ( $CHCl_3$ ), acetonitrile (ACN), dimethyl formamide (DMF), ethanol (EtOH), dimethyl sulfoxide (DMSO), and water. After 15 h, the samples were removed from the solvent, placed on a paper towel to remove excess solvent, and the length and width were measured. The volume of the sample was calculated and a ratio of the volume ( $V_t$ ) versus the initial volume ( $V_0$ ) of the sample was determined ( $V_t/V_0$ ). All measurements were made

**SCHEME 1:** Synthesis of Neutral (2), p-Doped (3), and de-Doped (4) Poly([3-VImC<sub>10</sub>O-4-MThienyl<sup>+</sup>][Br<sup>-</sup>]) from [3-VImC<sub>10</sub>O-4-MThienyl<sup>+</sup>][Br<sup>-</sup>] Ionic Liquid Monomer (1)

under ambient laboratory conditions: 21 °C ( $\pm 1$  °C), 53% ( $\pm 3$ %) relative humidity.

## Results and Discussion

The synthesis of the IL monomer, 1-(10-(4-methylthiophen-3-yloxy)decyl)-3-vinylimidazolium bromide, [3-VImC<sub>10</sub>O-4-MThienyl<sup>+</sup>][Br<sup>-</sup>], (1), was carried out in a multistep procedure as previously described.<sup>13,16</sup> Briefly, the monomer is synthesized in three steps (Scheme 1). In the first step, 3-methoxy-4-methylthiophene is prepared by the Cu(I)-catalyzed methoxylation of 3-bromo-4-methylthiophene.<sup>14</sup> In the second step, the decyl chain is introduced by reaction with bromodecanol. The product is then obtained by carrying out a quaternization reaction with vinyl imidazole. The synthesis, purification, and characterization of the monomer are more fully described elsewhere.<sup>13</sup>

The DSC heating scan collected on the dried monomer (1) over the range  $-65$  °C → 100 °C shows an endothermic phase transition with a peak maximum at 75.4 °C which is assigned to the ionic liquid melting point,  $T_m$  (Figure 1A). A  $T_m$  below 100 °C allows this monomer to be classified as an ionic liquid. It is noted that in addition to the melting point, a glass transition,  $T_g$ , is observed in the cooling curve with a midpoint transition at  $-16.3$  °C. The melting point determined for the bifunctional, vinyl thienyl IL monomer is 8 °C less than that determined for the corresponding methyl thienyl IL monomer.<sup>12</sup> The observed reduction in  $T_m$  upon replacement of the methyl moiety with

vinyl is consistent with prior work showing that introduction of an unsaturated side chain onto an imidazolium cation can serve to lower the melting point.<sup>17</sup> Additional information regarding the thermal properties of the IL monomer was obtained by fast scan (10 °C/min) thermogravimetric analysis (TGA) carried out under nitrogen atmosphere (Figure 1B). The monomer shows a single-step decomposition profile with an onset at 256.0 °C and a midpoint at 314 °C (Figure 1B). Decomposition to volatile products is almost complete at 400 °C with < 5 wt % sample remaining. It is noted that the bifunctional monomer decomposition onset is  $\sim 11$  °C higher and the midpoint is  $\sim 50$  °C higher than the corresponding methyl thienyl monomer.<sup>18,19</sup> The observed increase in the thermal decomposition temperature,  $T_d$ , of the vinyl substituted monomer over the methyl is consistent with that determined for methyldecylimidazolium chloride ( $T_d$  onset = 227 °C) and vinyldecylimidazolium chloride ( $T_d$  onset = 246 °C) ILs.<sup>10</sup>

Similar to other amphiphilic ILs, here too the monomer (1) can be self-assembled with the addition of water, forming an ordered (birefringent) lyotropic mesophase (Figure 2A).<sup>8–10,12,20</sup> At 18–20 (w/w) % total water content, the sample was a uniform, opaque, waxy solid at room temperature and displayed optical birefringence under polarized light (Figure 2A). Upon mild heating to 50 °C the mixture remains uniform but becomes a transparent liquid. The self-assembled structure of the binary mixture was examined by SAXS (Figure 2B). The scattering

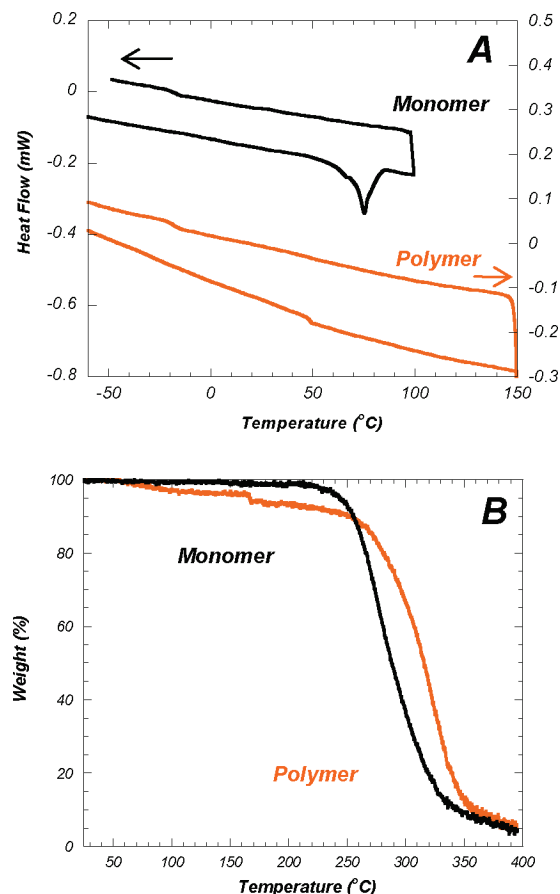


**Figure 1.** (A) DSC heating and cooling scan ( $2\text{ }^{\circ}\text{C}/\text{min}$ ) collected on dried, solid [ $3\text{-VImC}_{10}\text{O-4-MThienyl}^{+}\text{Br}^{-}$ ], black curve (left axis) and poly([ $3\text{-VImC}_{10}\text{O-4-MThienyl}^{+}\text{Br}^{-}$ ]), orange curve (right axis). (B) Fast scan ( $10\text{ }^{\circ}\text{C}/\text{min}$ ) TGA collected on [ $3\text{-VImC}_{10}\text{O-4-MThienyl}^{+}\text{Br}^{-}$ ], black curve and poly([ $3\text{-VImC}_{10}\text{O-4-MThienyl}^{+}\text{Br}^{-}$ ]), orange curve, both carried out under a  $\text{N}_2$  atmosphere.

pattern shows a broad correlation peak at  $q = 0.173\text{ \AA}^{-1}$  and a large hump of diffuse scattering in the high  $q$  region, consistent with a weakly ordered system.

Radical polymerization of the self-assembled binary mixture was carried out using a water-soluble azo initiator, A1BA, and heating the mixture to  $85\text{ }^{\circ}\text{C}$  (Scheme 1). The as-synthesized (neutral thiophene) polymer is a brownish-orange, self-supporting, and mechanically durable material (Figure 2C, left). The water content and thermal properties of the polymer were characterized by TGA and DSC (Figure 1). The TGA profile shows that the polymer is more thermally stable than the monomer. Specifically, the polymer shows a  $24.7\text{ }^{\circ}\text{C}$  increase (from  $314.5$  to  $339.2\text{ }^{\circ}\text{C}$ ) in the decomposition onset temperature. Here too, near complete loss of the sample is observed at  $400\text{ }^{\circ}\text{C}$ . The DSC thermograms collected on the second heating and cooling scans (Figure 1A) are devoid of any first-order phase transitions, confirming complete loss of the monomer. A secondary phase transition, a glass transition ( $T_g$ ), is observed in the cooling scan with a midpoint positioned at  $-18.5\text{ }^{\circ}\text{C}$ .

The determined gel fraction for the neutral form of the polymer was  $0.978 \pm 0.009$ . The high percentage of gel (97.8%) indicates that the polymer is well cross-linked, possessing a low amount of sol molecules.<sup>15</sup>

**Molecular Structure.** The as-synthesized polymer was characterized by ATR-FT-IR spectroscopy (Figure 3) and possesses characteristic modes indicating successful polymer-

ization of both the vinyl and thienyl moieties. Polymerization through the vinyl moiety positioned on the imidazolium was confirmed by the absence of both the  $970$  and  $910\text{ cm}^{-1}$   $\nu(\text{C}=\text{CH}_2)$  bands (Figure 3A).<sup>10</sup> Polymerization of the thiophene is demonstrated in part by the loss of the monomer aromatic  $\nu(\text{C}_\alpha-\text{H})$  stretching modes<sup>21</sup> at  $3037$  and  $788\text{ cm}^{-1}$  and the appearance of bands at  $3242$  and  $3131\text{ cm}^{-1}$  representing the  $\text{C}_\beta-\text{H}$  stretching vibrations.<sup>22</sup> The latter modes are often associated with a low molecular polythiophene or the presences of nonconventional cross links.<sup>23</sup> The spectrum also contains a mode at  $3076\text{ cm}^{-1}$  assignable to the aromatic  $\nu(\text{C}-\text{H})$  modes of the polythiophene.<sup>24</sup> The emergence of a mode at  $1680\text{ cm}^{-1}$  ( $\text{C}=\text{C}$  thienyl stretching vibration) confirms the 2,5 disubstitution of the thiophene rings in the polymer (Figure 3B).<sup>25</sup> The bands between  $1280$  and  $1200\text{ cm}^{-1}$  are assigned to the antisymmetric in-plane deformations,  $\delta_\alpha(\text{C}-\text{H})$ , and inter-ring stretching,  $\nu(\text{C}-\text{C})$ .<sup>24</sup> The mode at  $1163\text{ cm}^{-1}$  is assigned to the thiophene in-plane aromatic C-H stretch.<sup>26</sup> The  $770\text{ cm}^{-1}$  mode is characteristic of an  $\alpha,\alpha'$ -coupled alkyl-substituted polythiophene ring, suggesting a linear polymer chain structure.<sup>27</sup> It is noted that the apparent successful polymerization of the thienyl moiety employing the current synthetic approach was unexpected. The mechanism is believed to involve the oxidative polymerization of the thiophene moiety mediated by the growing A1BA initiated vinyl imidazolium dimer radical.<sup>28</sup> This mechanism is made favorable by the thiophene stacking. Further details regarding the mechanism of the polymerization are currently under investigation and will be reported elsewhere.<sup>29</sup>

The p-doped polymer was prepared by chemical oxidation achieved by suspending the polymer in an aqueous solution of  $\text{FeCl}_3$  (4 h) followed by addition of an aqueous solution of  $(\text{NH}_4)_2\text{S}_2\text{O}_8$  for 24 h (Scheme 1). This procedure produced a red-colored polymer (Figure 2C, center). In the presence of the oxidants, the polymer remains p-doped, however, upon removal of the oxidants the polymer reduces (within hours) back to a de-doped (neutral thiophene) state. The conversion of the polymer back to the neutral state in air (reduced by water in the air) is consistent with that previously reported for many polyalkylthiophenes which are thermodynamically more stable in the neutral state.<sup>30</sup> Changes in the FT-IR spectrum after oxidation confirm, in part, formation of the p-doped polymer. The oxidation of the polymer was evidenced by the appearance of bands at  $1046$  and  $974\text{ cm}^{-1}$  and the loss of modes at  $1394$ ,  $1263$ , and  $1224\text{ cm}^{-1}$ .<sup>12,31</sup>

The de-doped polymer was prepared by suspension of the oxidized solid polymer in an ethanolic solution of hydrazine for 15 h, yielding a deep green polymeric rod (Figure 2C, right). The de-doped form of the polymer possesses characteristic modes in the FT-IR spectrum (Figure 3), including the appearance of modes  $996$ ,  $1019$ ,  $1089$ , and  $1589\text{ cm}^{-1}$ .<sup>31</sup> In addition, several modes previously observed in the as-synthesized form of the polymer located at  $1679$  and  $1068\text{ cm}^{-1}$  are lost.<sup>31</sup> Furthermore, several observable modes occurring around  $3000\text{ cm}^{-1}$  are found to shift to higher wavenumbers after de-doping (Figure 3C).<sup>31</sup>

**Solvent Interactions.** The swelling behavior of the as-synthesized poly[ $3\text{-VImC}_{10}\text{O-4-MThienyl}^{+}\text{Br}^{-}$ ] in a variety of solvents was evaluated (Figure 4). A photo comparing the physical appearance of the dried and ethanol exposed polymer is presented in Figure 4A. A more complete examination of the swelling characteristics of the polymer was carried out by determination of the equilibrium volume swelling ratio ( $V/V_0$  at  $t_i = 15\text{ h}$ ) in solvents selected over a wide range of (Hansen) solubility parameters (Figure 4B). The Hansen solubility

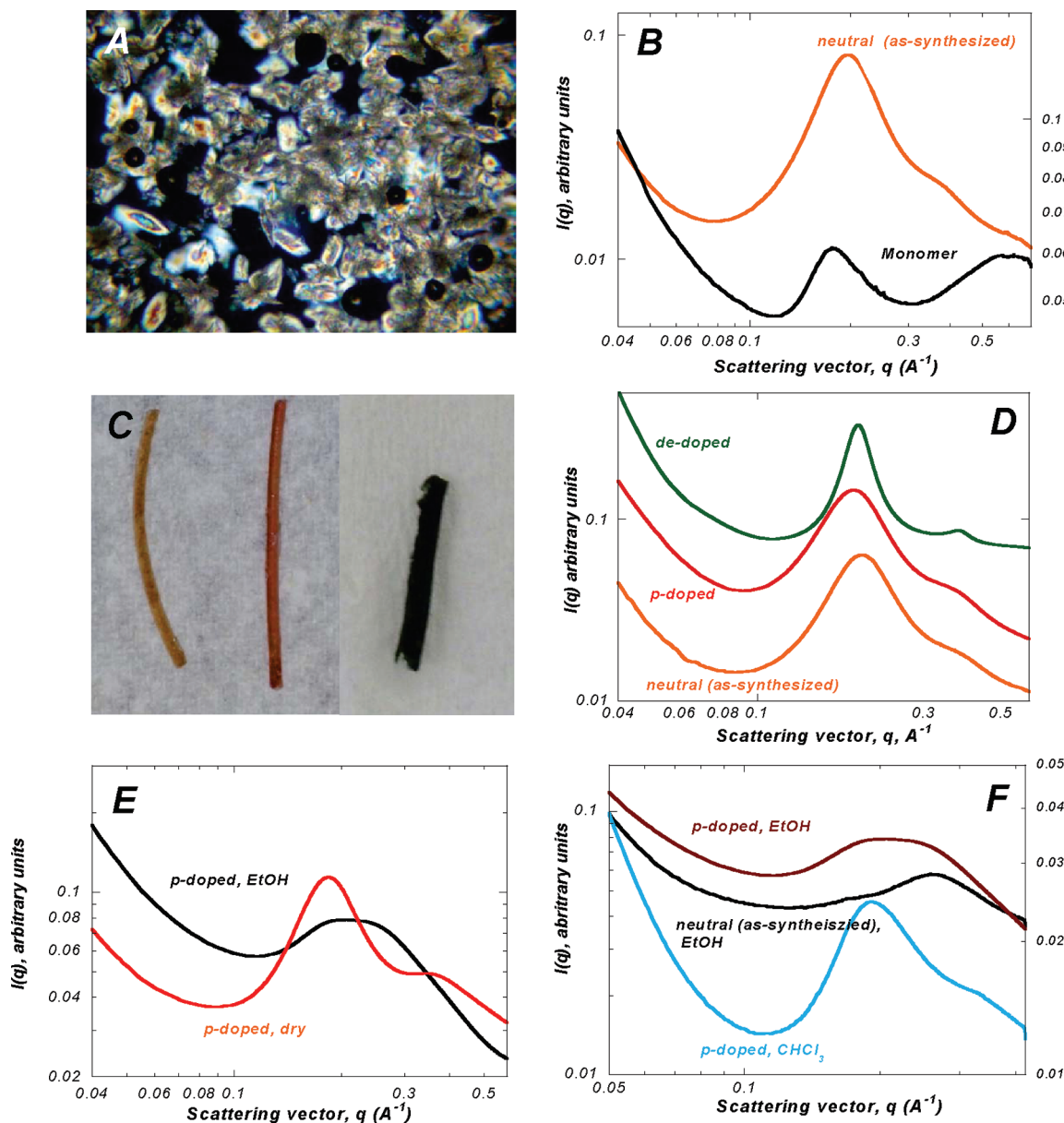


**Figure 2.** (A) Polarized optical micrograph of  $[3\text{-VImC}_{10}\text{O-4-MThienyl}^+]\text{[Br}^-]$  monomer in 20% (w/w) water. (B) SAXS profiles collected on  $[3\text{-VImC}_{10}\text{O-4-MThienyl}^+]\text{[Br}^-]$  monomer in 20% (w/w) water, black curve and as-synthesized poly( $[3\text{-VImC}_{10}\text{O-4-MThienyl}^+]\text{[Br}^-]$ ), orange curve. (C) Photograph of poly( $[3\text{-VImC}_{10}\text{O-4-MThienyl}^+]\text{[Br}^-]$ ) in as-synthesized (neutral thiophene), p-doped, and de-doped forms. (D) SAXS data collected on as-synthesized (neutral thiophene), p-doped, and de-doped forms of poly( $[3\text{-VImC}_{10}\text{O-4-MThienyl}^+]\text{[Br}^-]$ ). (E) SAXS data collected on p-doped dried and ethanol-solvated poly( $[3\text{-VImC}_{10}\text{O-4-MThienyl}^+]\text{[Br}^-]$ ). (F) SAXS data collected on as-synthesized (neutral thiophene) poly( $[3\text{-VImC}_{10}\text{O-4-MThienyl}^+]\text{[Br}^-]$ ) in ethanol and in the p-doped state in ethanol and chloroform.

parameter ( $\delta$ ) is a three-dimensional parameter dividing the total Hildebrand value into three parts, a dispersion force component,  $\delta_d$ , a polar component (dipole–dipole),  $\delta_p$ , and a hydrogen bonding component,  $\delta_h$ . Previously it has been shown that the swelling ratio will reach a maximum when the solubility parameter of the polymer ( $\delta$ ) matches the solvent.<sup>32</sup> As shown in Figure 4B, poly( $[3\text{-VImC}_{10}\text{O-4-MThienyl}^+]\text{[Br}^-]$ ) did not exhibit significant swelling in any of the solvents studied with swelling ratios,  $V_t/V_o$ , ranging only from 0 → 1.47 from hexane to water. The minimal swelling observed here suggests either a high degree of polymerization or cross linking. The low observed low swelling ratio is consistent with the determined high gel fraction (0.956 in xylene). Maximum swelling, (20% volume expansion) was achieved in chloroform with a  $\delta$  value of 19.0 MPa<sup>1/2</sup>. This provides an estimation of the solubility parameter for the polymer and indicates that the polymer is less polar than that determined for poly(AcrC<sub>8</sub>mim<sup>+</sup>)[Cl<sup>-</sup>], where

maximum swelling was observed to occur in highly polar solvents such as water and ethanol.<sup>8</sup> The lower polarity for poly( $[3\text{-VImC}_{10}\text{O-4-MThienyl}^+]\text{[Br}^-]$ ) may be attributed to polymerization through both the headgroup (vinylimidazolium) and tail region (alkyl chain-appended thiophene) of the monomer.

**Polymer Structure.** SAXS was used to determine the polymer nanostructure. The integrated data collected on the as-synthesized, dried polymer shows two broad diffraction peaks, the (100) at  $q = 0.198 \text{ \AA}^{-1}$  and the (200) at  $q = 0.394 \text{ \AA}^{-1}$ , indicating a lamellar structure with a d-spacing of 3.17 nm (Figure 2B). The absence of additional diffraction peaks in the high  $q$ -region of the scattering pattern indicates a lack of short-range ordering in the polymer. The p-doped, dried polymer possesses a similar SAXS pattern with only a slight increase ( $\sim 2 \text{ \AA}$ ) in the d-spacing observed (Figure 2D). The de-doped, dried polymer SAXS profile also shows two Bragg peaks in the low  $q$ -region ( $q = 0.194, 0.376 \text{ \AA}^{-1}$ ) but significant

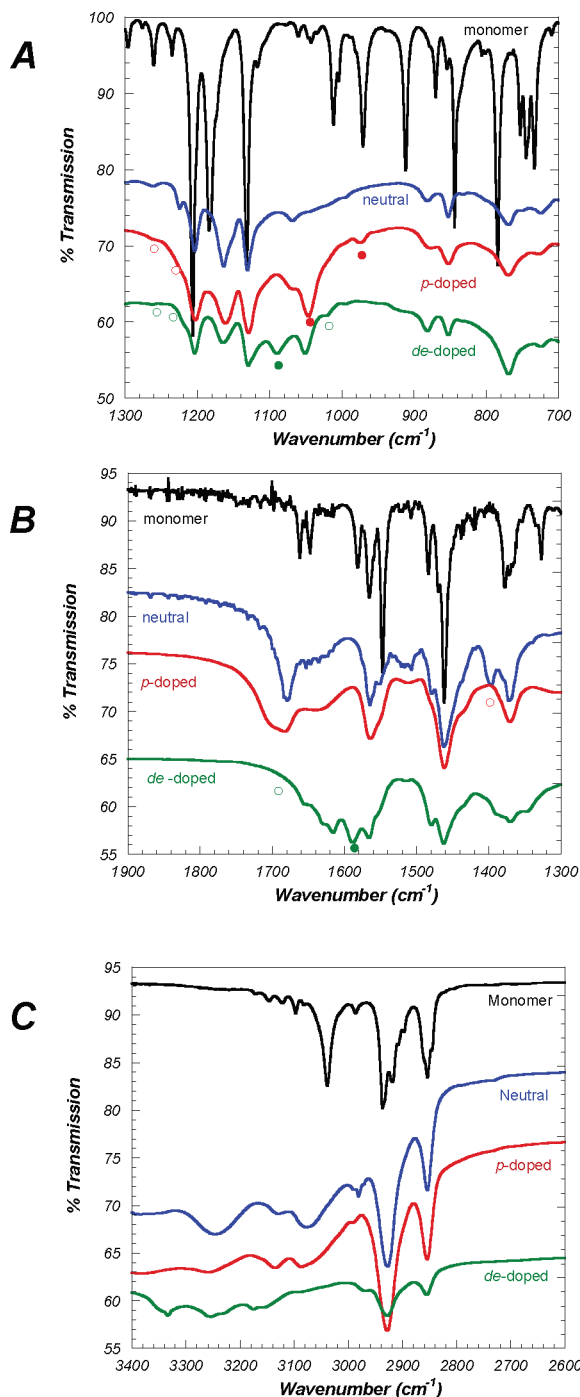


**Figure 3.** ATR-FT-IR spectra of solid  $[3\text{-VImC}_{10}\text{O-4-MThienyl}^+]\text{[Br}^-]$ , (black curve) and neutral (blue curve), p-doped (red curve) and de-doped (green) poly( $[3\text{-VImC}_{10}\text{O-4-MThienyl}^+]\text{[Br}^-]$ ) in the (A)  $1300\text{--}700\text{ cm}^{-1}$ , (B)  $1900\text{--}1300\text{ cm}^{-1}$ , and (C)  $3400\text{--}2500\text{ cm}^{-1}$  regions. Closed circles are used to indicate key vibrational modes that appear. Open circles indicate key vibrational modes lost.

narrowing of the diffraction peaks is observed, indicative of enhanced structural coherence (Figure 2D). The improved structural ordering observed after oxidation and reduction (p-doping and de-doping) of the polymer has been observed previously on solution cast polyalkylthiophenes (PATs) and has been used as an ordering tool for improving structure and transport properties in PATs.<sup>33</sup>

SAXS was also used to examine the influence of contacting the polymer with various solvents. In Figure 2E, the scattering patterns obtained on a dried, p-doped polymer is compared to

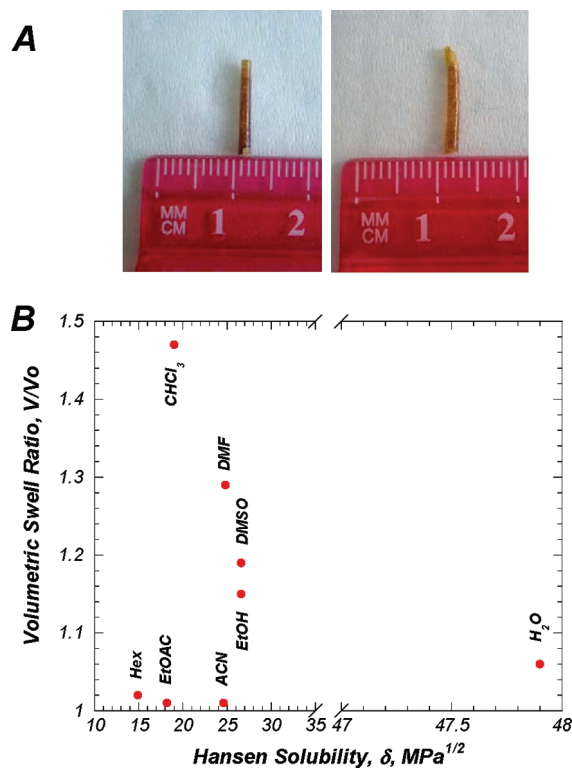


**Figure 4.** (A) Photograph of dried, as-synthesized (neutral thiophene), poly( $[3\text{-VImC}_{10}\text{O-4-MThienyl}^+]\text{[Br}^-]$ ), left image, and after soaking in ethanol for 15 h, right image. (B) Equilibrium volume changes ( $V/V_0$ ) of as-synthesized (neutral thiophene), poly( $[3\text{-VImC}_{10}\text{O-4-MThienyl}^+]\text{[Br}^-]$ ) as a function of Hansen solubility parameter evaluated for a range of organic solvents and water after 15 h of incubation.

a polymer fiber contacted with ethanol. The SAXS pattern collected on the ethanol-solvated p-doped polymer displays a single broad feature composed of two peaks [Gaussian peak fitting was performed using Igor Pro software (WaveMetrics Inc., Lake Oswego, OR)] positioned at  $q = 0.183$  and  $0.25\text{ \AA}^{-1}$  ( $\sqrt{1}, \sqrt{2}$ ), indicating the emergence of a discrete cubic phase. Additional details regarding the structure are unattainable due to the lack of any higher order diffraction features. The scattering pattern collected on chloroform contacted p-doped polymer can be deconvoluted into three diffraction peaks located at  $q = 0.182, 0.212, 0.286\text{ \AA}^{-1}$ , which can be indexed to the (211), (220), and (321) reflections of a bicontinuous cubic phase with  $Im\bar{3}m$  space group symmetry (Figure 2F).<sup>9</sup> The bicontinuous morphologies have been reported previously for other systems including poly(IL)s and are often found to occur as intermediate phases in systems transitioning between lamellar and discrete cubic phases. The scattering pattern collected on the as-synthesized (neutral) polymer in an ethanol-solvated state adopts a weakly ordered 2D hexagonal structure (Figure 2F) with peaks positioned at  $q = 0.155$  and  $0.269\text{ \AA}^{-1}$  ( $\sqrt{1}, \sqrt{3}$ ). Thus, it is postulated that the transition to the higher symmetry cubic phase in the p-doped polymer may arise from a combination of preferential solvation of the polyalkylthiophene backbone and the formation of the partial quinoid geometry (increased double bond character of the thiophene inter-ring) of the thiophene upon oxidation, a state which has been previously believed to reduce conformational disorder.<sup>33</sup>

**Electronic Transport.** The conductivity for the as-synthesized polymer was determined to be  $4.7 \times 10^{-7}\text{ S/cm}$ . The value is considerably lower than typically observed for many polyalkylthiophenes. For comparison the conductivity of rrP3HT

films are on the order of  $10^{-5}$  S/cm.<sup>34</sup> In the p-doped state, the conductivity value for the poly[3-VImC<sub>10</sub>O-4-MThienyl<sup>+</sup>][Br<sup>-</sup>] did increase to  $9.8 \times 10^{-5}$  S/cm. The values determined for both the as-synthesized and p-doped forms of the polymer are lower than that attainable by electropolymerization of the bifunctional monomer, which were found to be 0.53 and 2.36 S/cm, respectively.<sup>13</sup> The poor conductivity determined for the polymer prepared from radical initiated polymerization of the self-assembled lyotropic mesophase most likely arises from the poor structural ordering/coherence as determined by SAXS.<sup>35–37</sup>

**Optical Characteristics.** The optical properties of the solid polymer were determined and compared to the monomer in Figure 5. The UV-vis spectrum collected on the [3-VImC<sub>10</sub>O-4-MThienyl<sup>+</sup>][Br<sup>-</sup>] monomer (Figure 5A, blue curve) is featureless in the 265–800 nm region, an observation consistent with the white appearance of the solid. The large absorption below 265 nm arises from the charge-transfer band of the imidazolium functionality.<sup>12,13</sup> The UV-vis spectrum collected on dried (black curve) and ethanol-solvated (red curve) as-synthesized (neutral thiophene) polymer are compared in Figure 5A. The dried, neutral state polymer spectrum shows two additional peaks not observed in the monomer spectrum positioned at ca. 300 and a smaller, broader peak at 340 nm. The absorption features are assigned to the  $\pi-\pi^*$  transition of the extended  $\pi$ -electron system. It is noted that the peak maximum is blue-shifted relative to that observed for poly[thienylC<sub>10</sub>MIm<sup>+</sup>]<sub>2</sub>[SO<sup>2-</sup>] ( $\lambda_{\text{max}} = 391$  nm) and poly[3-VImC<sub>10</sub>O-4-MThienyl<sup>+</sup>][Br<sup>-</sup>] produced by electropolymerization ( $\lambda_{\text{max}} = 380$  nm).<sup>12,13</sup> Upon immersion of the solid polymer rods in ethanol an absorption band located at 343 nm becomes pronounced. The increased prominence and red shifting of the  $\pi-\pi^*$  transition signals an increase in the effective conjugation length of the polythiophene backbone (i.e., reduced twisting). It has been previously noted that an increase in the effective conjugation length can serve to increase coplanarity between neighboring polythiophene chains.<sup>38</sup> For example, the presence of various anions on the absorption spectra of aqueous solutions of cationic polythiophenes have been studied and were found to red shift the absorption bands, due to anion-induced aggregation and concomitant planarization of the polymer.<sup>39</sup> Thus, the observed red shifting in the absorption bands suggest that ethanol solvation of the polymer chains serve to stabilize a more planar configuration of the polythiophene backbone relative to that achieved in the dried, as-synthesized (neutral) state.<sup>40</sup>

The UV-vis spectra collected on freshly oxidized, dried and ethanol soaked polymer are presented in Figure 5B. The dried, p-doped polymer spectrum contains an absorption band not observed in the dried, as-synthesized (neutral) form at 421 nm. The redox-induced changes in the polymer optical spectrum have been previously reported for the electropolymerized polymer.<sup>13</sup> As the polymer is oxidized a reduction in the  $\pi-\pi^*$  transition band characteristic of the neutral form and concomitant appearance of new absorption bands, signaling the formation of polaron charge carriers is observed. Here, the dried, oxidized polymer shows coexistence of the  $\pi-\pi^*$  band associated with the neutral form, indicating that the p-doped state is not fully retained upon removal from the oxidants. The spectrum recorded for the p-doped, ethanol-solvated polymer reveals an additional absorption band at 512 nm. The presence of two absorption bands in the p-doped ethanol-solvated state may suggest the coexistence of two species with the more intense 512 nm band comprising the dominant component. Recently, Yamamoto et al. has shown that  $\pi$ -stacked conjugated polymers can form stable colloidal particles in chloroform and methanol solutions,

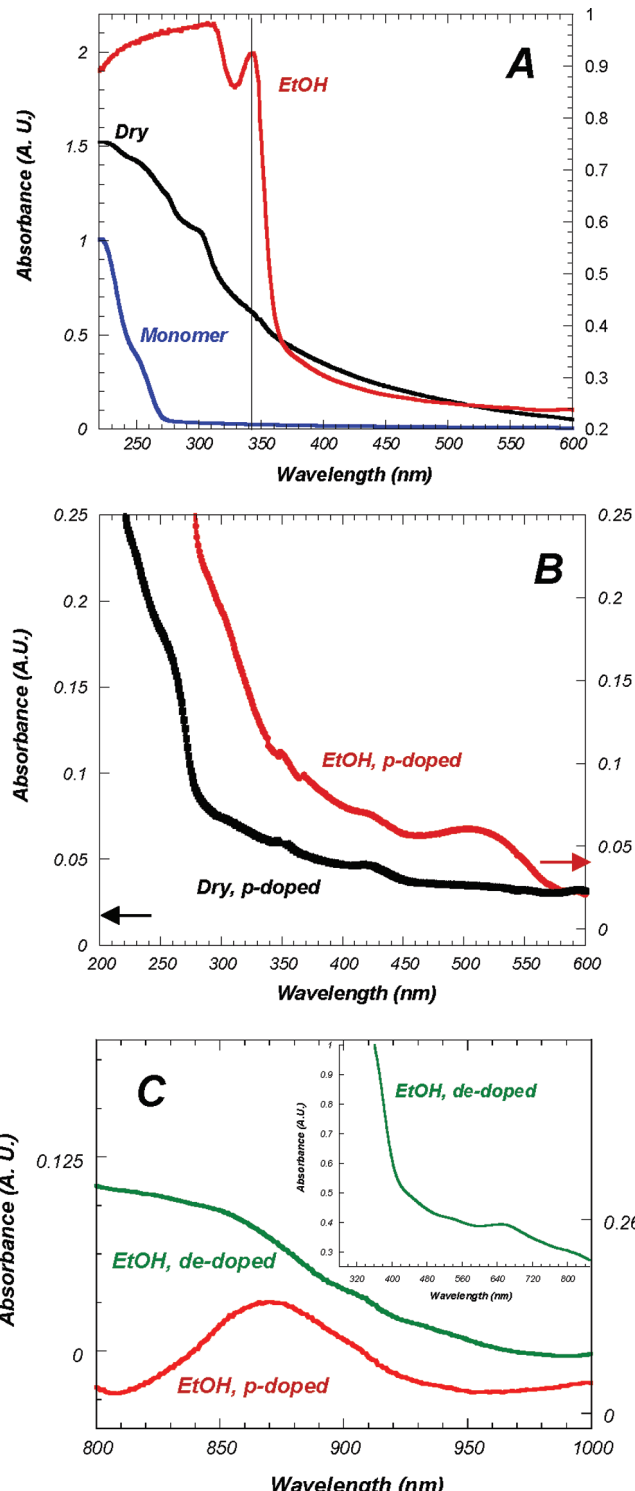


**Figure 5.** (A) UV-vis absorption spectra recorded on monomer (blue curve, right Y-axis) and polymer in dried, as-synthesized (neutral thiophene), state (black curve, right Y-axis), and ethanol-solvated state (red curve, left Y-axis). (B) UV-vis absorption spectra of polymer in dried, p-doped state (black curve, left Y-axis) and ethanol-solvated state (red curve, right Y-axis). (C) Vis-NIR absorption spectra of polymer in ethanol-solvated p-doped (red curve, left Y-axis) and de-doped (green curve, right Y-axis) states and de-doped ethanol-solvated state UV-vis (green, inset). Measurements made on the dried polymers used multiple fibers aligned within a 1 mm delaminated quartz cuvette or in a 5 mm square quartz cuvette.

producing large, higher-order aggregated structures that preferentially adopt a cubic packing arrangement.<sup>41</sup> Thus, it is possible that the emergence of the band at 512 nm may signal

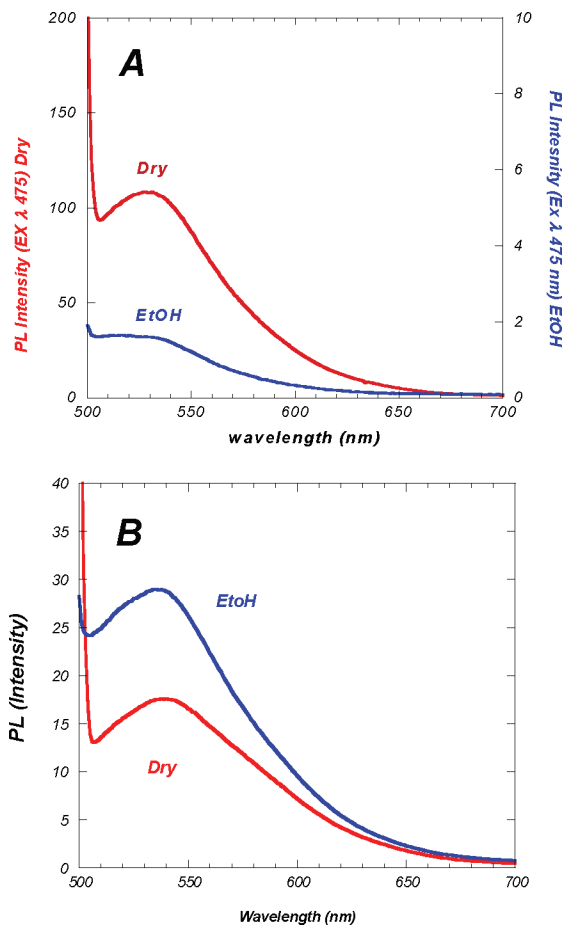


**Figure 6.** (A) Photoluminescence spectra recorded on dried (red spectrum) and ethanol-solvated (blue spectrum) as-synthesized (neutral thiophene), poly([3-VImC<sub>10</sub>O-4-MThienyl<sup>+</sup>][Br<sup>-</sup>]) collected at 475 nm excitation wavelength. (B) Photoluminescence spectra recorded on dried (red spectrum) and ethanol swollen (blue spectrum) p-doped poly([3-VImC<sub>10</sub>O-4-MThienyl<sup>+</sup>][Br<sup>-</sup>]) collected at 475 nm excitation wavelengths. All measurements made on a bundle of cylindrical polymers loaded into a 5 mm quartz cuvette.

the formation of a population of such aggregates. Additional scattering studies will be required to fully determine if the appearance of the 512 nm band in the solvated p-doped polymer arises from the formation of cubic-packed aggregates. The NIR spectral region recorded on the ethanol-solvated p-doped polymer (Figure 5C, red curve) contains the expected bipolaronic band centered at 870 nm.<sup>13</sup> Finally, formation of the de-doped polymer can be achieved by treating the oxidized ethanol-solvated polymer with hydrazine. The UV-vis spectrum recorded on the de-doped, ethanol-solvated polymer is presented in Figure 5C, inset. The bipolaronic band in the NIR spectrum is found to vanish (Figure 5C, green curve) and an absorbance band occurs at 655 nm, which is often ascribed to the  $\pi-\pi^*$  electronic transition of de-doped conjugated polymers.<sup>42</sup>

The photoluminescence (PL) of conjugated polymers is dependent upon the geometry of the polymer backbone and the polymer chain aggregation state. For example, the PL intensity of aggregated polythiophene derivatives compared with those in a single chain state has been shown to be weaker by approximately 1 order of magnitude. The PL spectra recorded on dried and ethanol exposed polymer fibers in the as-synthesized (neutral thiophene) state are presented in Figure 6A. The steady-state fluorescence spectrum recorded on the polymer (excited with 475 nm light) in the dried state exhibits emission considerably greater in intensity (nearly 2 orders of magnitude)

than polymer in ethanol. The broad emission band maximum is at 529 nm. A large Stokes shift, that is, the difference between the wavelength of the absorption maximum and the maximum of the emission band is observed. The large Stokes shift is an additional indicator that the polymer backbone in this state (dried, neutral form) is highly twisted.<sup>12</sup> Thus, the enhanced PL intensity for the dried, neutral form of the polymer suggests that it lacks the required configuration for formation of strong interchain interactions. Upon ethanol solvation, the as-synthesized (neutral thiophene) polymer emission intensity decreases (reduced quantum yield) and broadens. The reduced PL intensity suggests the presence of strong intermolecular interactions between thiophene polymer chains mediated by solvent induced spatial reorganization of the polymer backbone.<sup>43,44</sup> It is noted that the polymer in both the dried and ethanol-solvated states show wavelength dependent changes in the emission spectra collected at a range of excitation wavelengths (425 → 475 nm).

An opposite trend is observed for the PL spectra recorded on the chemically oxidized polymer (Figure 6B). Specifically, samples exposed to ethanol show higher emission intensity than those in the dried state. It is noted here, however, that the difference between dried and ethanol-solvated polymer emission is not as great as that observed for polymers in the neutral form. The reduced emission intensity again signals close-packing of the polymer chains and possible aggregate formation. Exciting the ethanol swollen, p-doped polymer at 475 nm yields an emission spectrum with a broad (multicomponent) peak with a primary emission maximum at 535 nm (shoulder at 518 nm). Also noted is the reduction in the Stokes shift indicating decreased twisting of the conjugated segments and increased coplanarity. The PL spectra recorded on the dried, fully contracted p-doped polymer shows a maximum emission at 538 nm with 475 nm excitation. As observed for the neutral state of the thiophene polymer, exciting the sample at lower wavelengths (450, 425 nm) results in broadening of the emission peak with multiple components noted. The slight red shifting in the emission maximum in the dried versus ethanol-solvated p-doped polymer suggests an enhanced degree of planarization of the polymer in the dried state. Thus, when the polymer is ethanol-solvated the interplanar distance increases due to separation of the polythiophene backbone thus reducing the  $\pi-\pi$  interactions or interchain interactions and manifests as a blue shift in the peak emission and an increase in PL intensity.<sup>2</sup> While the polymer does not exhibit significant volume changes upon extended exposure to ethanol it does serve to solvate the polymer chains sufficiently to loosen interchain interaction, causing suppression in the emission intensity. The observed differences in the PL spectra recorded for the p-doped polymer compared to the neutral form may in part be explained by recent ab initio studies carried out on thiophene oligomers that found that  $\pi$ -stacking interactions in conjugated polymers can be turned on and off as a function of applied electrochemical potential (oxidation state).<sup>45</sup> More specifically, this work determined that parallel,  $\pi$ -stacked thiophenes in the neutral state are weakly interacting, but in the p-doped state the charged molecules electrostatically repel each other, overwhelming the  $\pi-\pi$  stacking between adjacent radical cations. Although more work is needed to more fully understand the relationship between oxidation state–polymer conformation and optical properties, the observed sensitivity of ionic liquid-based polythiophenes to variations in redox and solvation state may provide a means to either more fully optimize these properties or to allow for external regulation of them.

## Conclusions

Thermal, free-radical polymerization of a bifunctional IL monomer possessing both vinyl and thienyl groups self-assembled in water was demonstrated. Successful polymerization through both groups was evidenced by vibrational spectroscopy. The mechanism of the polymerization is not fully understood but is currently under investigation and will be detailed in a future report. The resultant polymer is a mechanically durable, self-supporting material that does not swell appreciably in either water or common organic solvents. In all oxidation states, the polymer adopts a weakly ordered lamellar structure in its dried form. Electrical conductivity is poor and is believed to originate from the lack of significant long and short-range structural ordering. Subjecting the polymer to ethanol serves to solvate the polymer chains in such a fashion to trigger a structural conversion to a weakly ordered nonlamellar phase (i.e., 2D hexagonal or cubic). The optical characteristics were found to be adjustable depending on polymer oxidation state and solvation conditions. In the as-synthesized (neutral thiophene) form, a blue shift of the absorption maximum and an increase in the PL emission intensity is observed in the dried state relative to the ethanol-solvated state. The observed changes in the optical characteristics indicate that the as-synthesized poly(thiophene) backbone planarity is enhanced upon ethanol solvation relative to that in the dried state. Conversely, in the p-doped state, the PL emission intensity is slightly suppressed in the dried state compared to the ethanol-solvated polymer. The inversion in behavior compared to the neutral state polymer is attributed to a combination of oxidation-state-induced changes in the  $\pi$ -stacking interactions and solvent-induced interchain interactions. Future work more closely examining the aggregate structure formed upon ethanol solvation of the p-doped polymer will be carried out. It is anticipated that by understanding the subtle oxidation and solvent induced inter- and intrachain conformational/structural changes, fine-tuning and optimization of the photophysical characteristics of the polymer can be achieved, allowing for dynamic tuning of the emission properties. More importantly, this work demonstrates the possibility of designing a conjugated polymer where reversible control over the structure (nanoscopic order/disorder) can offer a simple means by which to control the optical/photophysical properties of a  $\pi$ -conjugated polymer. Understanding how to control hierarchical structure in conjugated materials is important for their ability to be used for a wider variety of optoelectronic applications.

**Acknowledgment.** This work was supported by the Office of Basic Energy Sciences, Division of Materials Sciences, United States Department of Energy under Contract No. DE-AC02-06CH11357 to the UChicago, LLC.

## References and Notes

- (1) Moliton, A.; Hiorns, R. *Polym. Int.* **2004**, *53*, 1397–1412.
- (2) Li, Y. N.; Vamvounis, G.; Holdcroft, S. *Macromolecules* **2002**, *35*, 6900–6906.
- (3) Zhang, B.-z.; Zhao, X.-y. *J. Mater. Sci.* **2009**, *44*, 2765–2773.
- (4) Faid, K.; Leclerc, M. *J. Am. Chem. Soc.* **1998**, *120*, 5274–5278.
- (5) Jiang, H.; Taranekar, P.; Reynolds, J. R.; Schanze, K. S. *Angew. Chem., Int. Ed.* **2009**, *48*, 4300–4316.
- (6) Dufresne, G.; Bouchard, J.; Belletete, M.; Durocher, G.; Leclerc, M. *Macromolecules* **2000**, *33*, 8252–8257.
- (7) Bouchard, J.; Belletete, M.; Durocher, G.; Leclerc, M. *Macromolecules* **2003**, *36*, 4624–4630.
- (8) Batra, D.; Hay, D. N. T.; Firestone, M. A. *Chem. Mater.* **2007**, *19*, 4423–4431.
- (9) Batra, D.; Seifert, S.; Firestone, M. A. *Macromol. Chem. Phys.* **2007**, *208*, 1416–1427.
- (10) Batra, D.; Seifert, S.; Varela, L. M.; Liu, A. C. Y.; Firestone, M. A. *Adv. Funct. Mater.* **2007**, *17*, 1279–1287.
- (11) Grubjesic, S.; Seifert, S.; Firestone, M. A. *Macromolecules* **2009**, *42*, 5461–5470.
- (12) Burns, C. T.; Lee, S.; Seifert, S.; Firestone, M. A. *Polym. Adv. Technol.* **2008**, *19*, 1369–1382.
- (13) Lee, S.; Becht, G. A.; Lee, B.; Burns, C. T.; Firestone, M. A. *Adv. Funct. Mater.* **2010**, *20*, 2063–2070.
- (14) Wang, S.; Kempen, D. H.; Simha, N. K.; Lewis, J. L.; Windebank, A. J.; Yaszemski, M. J.; Lu, L. *Biomacromolecules* **2008**, *9*, 1229–1241.
- (15) Nandi, S.; Winter, H. H. *Macromolecules* **2005**, *38*, 4447–4455.
- (16) Ho, H. A.; Bera-Aberem, M.; Leclerc, M. *Chem.—Eur. J.* **2005**, *11*, 1718–1724.
- (17) Min, G.-H.; Yim, T.; Lee, H. Y.; Huh, D. H.; Lee, E.; Mun, J.; Oh, S. M.; Kim, Y. G. *Bull. Korean Chem. Soc.* **2006**, *27*, 847–852.
- (18) Nakajima, H.; Ohno, H. *Polymer* **2005**, *46*, 11499–11504.
- (19) Ohno, H. *Macromol. Symp.* **2007**, *249*–*250*, 551–556.
- (20) Green, O.; Grubjesic, S.; Lee, S. W.; Firestone, M. A. *Polym. Rev.* **2009**, *49*, 339–360.
- (21) Cirpan, A.; Alkan, S.; Toppore, L.; Cianga, I.; Yagci, Y. *J. Mater. Sci.* **2002**, *37*, 1767–1775.
- (22) Louarn, G.; Buisson, J. P.; Lefrant, S.; Fischou, D. *J. Phys. Chem.* **1995**, *99*, 11399–11404.
- (23) Dams, R.; Vangeneugden, D.; Vanderzande, D. *Chem. Vap. Deposition* **2006**, *12*, 719–727.
- (24) Casado, J.; Hotta, S.; Hernandez, V.; Lopez Navarrete, J. T. J. *Phys. Chem. A* **1999**, *103*, 816–822.
- (25) Bhat, K.; Kumar, M. S. J. *Mater. Sci.* **2007**, *42*, 8158–8162.
- (26) Louarn, G.; Trznadel, M.; Buisson, J. P.; Laska, J.; Pron, A.; Lapkowski, M.; Lefrant, S. *J. Phys. Chem.* **1996**, *100*, 12532–12539.
- (27) Wang, C.; Benz, M. E.; LeGoff, E.; Schindler, J. L.; Allbritton-Thomas, J.; Kannewurf, C. R.; Kantzidis, M. G. *Chem. Mater.* **1994**, *6*, 401–411.
- (28) Yagci, Y.; Jockusch, S.; Turro, N. J. *Macromolecules* **2007**, *40*, 4481–4485.
- (29) Redfern, P.; Becht, G. A.; Curtiss, L. A.; Firestone, M. A. Argonne National Laboratory, Argonne, IL. Unpublished work.
- (30) Chun-Guey, W.; Mei-Jui, C.; Yii-Chung, L. *J. Mater. Chem.* **1998**, *8*, 2657–2661.
- (31) Kvarnstrom, C.; Neugebauer, H.; Ivaska, A.; Sariciftci, N. S. *J. Mol. Struct.* **2000**, *521*, 271–277.
- (32) Mutelet, F.; Butet, V.; Jaubert, J.-N. *Ind. Eng. Chem. Res.* **2005**, *44*, 4120–4127.
- (33) Apperloo, J. J.; Janssen, R. A. J.; Nielsen, M. M.; Bechgaard, K. *Adv. Mater.* **2000**, *12*, 1594–1597.
- (34) Lu, G.; Tang, H.; Qu, Y.; Li, L.; Yang, X. *Macromolecules* **2007**, *40*, 6579–6584.
- (35) Hassenkam, T.; Greve, D. R.; Bjørnholm, T. *Adv. Mater.* **2001**, *13*, 631–634.
- (36) Tran-Van, F.; Garreau, S.; Louarn, G.; Froyer, G.; Chevrot, C. *J. Mater. Chem.* **2001**, *11*, 1378–1382.
- (37) Kurata, T.; Mohri, T.; Takimiya, K.; Otsubo, T. *Bull. Chem. Soc. Jpn.* **2007**, *80*, 1799–1807.
- (38) Xu, B.; Holdcroft, S. *Macromolecules* **1993**, *26*, 4457–4460.
- (39) Ho, H. A.; Leclerc, M. *J. Am. Chem. Soc.* **2003**, *125*, 4412–4413.
- (40) Guey, C.-W.; Jui, M.-C. *J. Mater. Chem.* **1998**, *8*, 2657–2661.
- (41) Yamamoto, T.; Komarudin, D.; Arai, M.; Lee, B. L.; Suganuma, H.; Asakawa, N.; Inoue, Y.; Kubota, K.; Sasaki, S.; Fukuda, T.; Matsuda, H. *J. Am. Chem. Soc.* **1998**, *120*, 2047–2058.
- (42) Han, M. G.; Foulger, Stephen, H. *Small* **2006**, *2*, 1164–1169.
- (43) Kim, J. *Pure Appl. Chem.* **2002**, *74*, 2031–2044.
- (44) Yang, J.-S.; Swager, T. M. *J. Am. Chem. Soc.* **1998**, *120*, 5321–5322.
- (45) Scherlis, D. A.; Marzari, N. *J. Am. Chem. Soc.* **2005**, *127*, 3207–3212.